Calculating tortuosity in quasi-random anisotropic packings

Parvez Alam, Thomas Byholm and **Martti Toivakka,** Åbo Akademi University, Turku, Finland

KEYWORDS: Tortuosity, Coatings, Particles, Packings, Simulation, Random, Permeability, Porous

SUMMARY: Relating the micro-structural characteristics of porous media to their through-flow properties remains an interesting challenge for the paper coating community. The research presented herein attempts to address this challenge through computational science for complex quasi-random anisotropic plate-like particle packings. In plate-like packings comprising monodisperse plates of equal aspect ratios, tortuosity is seen to decrease as a function of porosity. However, tortuosity is concurrently found to increase as a function of increasing particle aspect ratio, even though the porosities of such packings are higher. Dimensional and rotational characteristics of plate-like packings are therefore seen to be more influential to tortuosity than volume fractions of pore space. When comparing tortuosity to mean tracer velocities, the generic trend is one of inverse proportionality, with higher levels of scatter existing at lower tracer velocities. It is postulated that nesting sites within the particle microstructure accounts for the lower velocities by effectively trapping the flow of fluid for discrete time periods, and reducing the total distances travelled through the packing. As a function of the mean spatial rotations, tortuosity is taken to be 2nd order. Inverse linear proportionality is found to exist between tortuosity and the D'Arcy permeability calculated for the packed media. Porosity tends to increase as a function of Euclidean spatial particle rotations.

ADDRESS OF THE AUTHOR(S): Parvez Alam (parvez.alam@abo.fi), **Thomas Byholm** (tbyholm@abo.fi) and **Martti Toivakka** (martti.toivakka@abo.fi): Åbo Akademi University, Faculty of Technology, Department of Chemical Engineering, Laboratory of Paper Coating and Converting, Porthaninkatu 3, FIN-20500 Åbo/Turku, Finland.
Corresponding author: Parvez Alam

Anfractuous pore-space microstructures are typically generated in particulate based materials such as paper coatings. The transfer of fluids through coatings is determined by the micro-structural characteristics of the material. Building the knowledge base that links the microstructure to fluid flux eccentricities is a stimulating challenge. Tortuous flow of fluids in particulate based coatings can influence key flux characteristics such as their spreading-imbibition distribution profiles. Additionally, the impact that coating microstructure has on properties like the permeability should be better understood as it is a critical determinant of moisture transfer to the underlying materials. Ultimately, tortuosity has an influence on important physical processes related to printing and papermaking. These include ink/fountain solution setting and absorption, vapour transfer through coatings, barrier properties and the drying mechanisms of paper coatings. Given the importance tortuosity has on the intra-structural mechanisms of fluid and gas motion, it is evidently under-researched in the paper coating community. This is no surprise since the interrelationships between particle size and shape, as well as the mass transfer properties of coatings are not trivial to predict. Nevertheless, overlapping ideas can be drawn from other fields of science where both experimental and computational research has been reported.

There is discrepancy in the literature as to the precise mathematical representation of tortuous flow. The root of each variant is not intended here, but rather a simple account of the different models and the model intended for use in this paper. The simplest model for tortuosity, τ, shall be the model used herein. This model, following Epstein (1989), states that $\tau = L_e/L$, where L_e is the total distance travelled through a packing and L is the shortest theoretical distance between a defined starting and a defined ending point. This model of tortuosity has been used widely (e.g. Koponen 1998; Dias et al. 2006) and $\tau \leq 1$. Researchers such as Kim and Chen (2006) and Maeriki et al. (2003) use a tortuosity factor, τ^2, which essentially arises from experimental requirements to calculate tortuosity. The means of arriving at the tortuosity factor relies on the theory of ion diffusion and electrical conductance in porous media used alongside electrical resistance measurements in the bulk and fluid materials. Bear (1972) explains this in detail arriving at $\tau^2 = (L/L_e)^2$ leading to $\tau \leq 1$ (note the inverse of the tortuosity, τ, described above if the square root is taken on both sides).

The tortuosity of packed media is rarely a constant value; rather, it varies according to factors related to both the motion of a fluid or gaseous material coupled with certain geometrical characteristics of the packing. Increasing particle sizes, for example, whilst maintaining a constant porosity has been shown by Petford and Koenders (2001) to reduce the tortuous flux of an incoming fluid. A decrease in tortuosity by a factor of around 100 was reported on an approximately five-fold increase in particle size. Seemingly contradicting research was conducted by Attia (2005) who showed that increasing the percentage of finer particles in a packing decreased the tortuosity of the packing bed. Attia's research however, did not fix the packing porosity, which typically becomes higher for finer particle packings, (Cumberland, Crawford 1987). Therefore Attia (2005) studied more realistic packing behaviour when varying the particle sizes as the resultant change in porosity was inclusive rather than controlled.

In a scientific comment by Boudreau (1996), various statistical models developed for sphere packings since the 1880's were shown to relate tortuosity as a non-linearly decreasing function of increasing porosity, φ. Dias et al. (2006) comparing with experimental data, considered the inverse power law function, $\tau = \varphi^{-n}$, to be the best fit for granular and spherical packings within the porosity range 0.4-0.5. Moreover, Kim and Chen (2006), using a random

walk simulation approach reveal a clearly non-linear fit of tortuosity on particle volume fraction (1 - φ) for both systematically packed and randomly distributed monodisperse spheres. This finding is further reinforced by spherical packing models developed by Zalc et al. (2004) and analytical models by Moldrup et al. (2001). In general, the majority of tortuosity-porosity relationships have assumed spherical particle geometries, with aspect ratios of unity. Non-spherical two-dimensional computational models using the lattice-gas simulation method, Koponen (1998), suggest linear inverse proportionality between the two parameters. Koponen suggests an empirical relationship of the form $\tau = 0.8(1 - \varphi) + 1$. Though Koponen also used geometries with aspect ratios equal to unity, the use of 2-dimensional squares rather than spheres may be one reason as to why a linear trend between tortuosity and porosity was observed. Nonetheless, the modelling of tortuosity in two dimensions rather than three may also contribute to the difference. Ultimately, a decreasing tortuosity as a function of increasing porosity (or decreasing particle volume fraction) is consistent in all of the suggested models.

Porosity alone does not explain tortuosity in packed particle structures. Pore and neck dimensions, shapes and their connections all intrinsically define the magnitude of the tortuous paths. Models developed by Armatas and Pomonis (2004) represented pores as cylindrical geometries making the assumption that pore diameters were equal to pore lengths ($d_p = l_p$). This assumption coincided with micrograph studies performed by Dullien (1992) who discerned this same phenomenon. Based on their models, Armatas and Pomonis (2004) stipulated that the presence of micro-pores in structures that otherwise have the same porosity and particle geometries, yields significantly higher values for tortuosity. Macro-pores have time-dependant effects on fluid ingress such that they raise the rapidity of filling at earlier times, after which the volume flux of fluid lessens, (Allaire-Leung et al. 2000). In later work, Armatas (2006) determines that the tortuosity factor is linked more closely to the standard deviation of the pore size distribution and less to the connectivity.

The long-term goals of this research are to accurately relate liquid flow characteristics through coatings to their unique microstructures. The achievement of these goals would allow for the design and optimisation of coatings to yield microstructure-specific properties, tailored to suit different applications. The ability to control the coating flow characteristics has many applications in industry including printing, adhesion and the development of barrier properties. This paper presents preliminary research findings that aim to focus tortuosity analyses to non-spherical plate-like particle packings. Plate-like packings can be considered homonymous to kaolin based coating structures. This first stage of research is further geared to determining whether or not concepts reported in the literature for spherical particle packings, are also valid for plate-like packings.

Method

Non-deformable quasi-random monodisperse plate-like particle packings were generated with aspect ratios of 6.52, 14 and 28 and were rotated in orthogonal Cartesian axes to a maximum of 40 degrees, *Figs 1-3*. The mean Euclidean spatial rotations for these packings were 22.3°, 22.4° and 20.3° respectively.

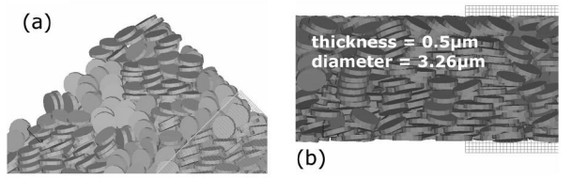

Fig 1. Plate-like packing using aspect ratios of 6.52 showing (a) a corner perspective and (b) a side view.

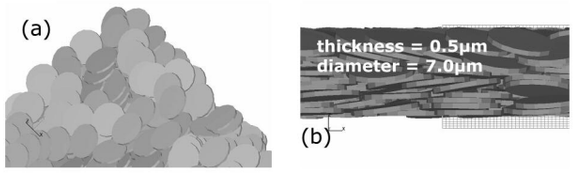

Fig 2. Plate-like packing using aspect ratios of 14 showing (a) a corner perspective and (b) a side view.

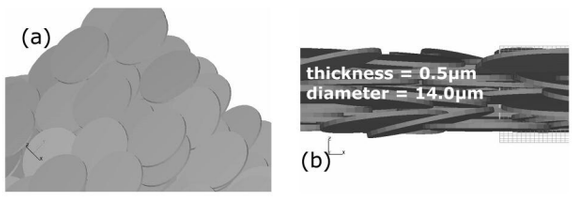

Fig 3. Plate-like packing using aspect ratios of 28 showing (a) a corner perspective and (b) a side view.

Six further plate-like packings, (a)-(f), were generated with aspect ratios of 6.52 (*radius* = 1.63 µm, *height* = 0.5 µm). In these packings the maximum axial rotations were varied between 0° and 45°. The maximum rotations allowed in each orthogonal axis, ω_{max}, the consequent mean spatial rotations, ω_t, (calculated using *Eq 1*) for each packing and the resulting porosities, φ, are given in *Table 1*. In *Eq 1*, *n*, is the sample number, *x*, *y* and *z* are the principle Cartesian axes. One monodisperse random spherical packing was also generated with a particle volume fraction equal to the plate packing simulations in series (a)-(f).

$$\omega_t = \left[\sum_i \sqrt{\omega_{x_i}^2 + \omega_{y_i}^2 + \omega_{z_i}^2} \right] \cdot n^{-1} \qquad [1]$$

Table 1. Maximum axial rotations, mean Euclidean spatial rotations and resulting porosities for packings with an aspect ration of 6.52 (*radius* = 1.63 µm, *height* = 0.5 µm).

	ω_{max} / °	ω_t / °	φ
a	0	0.0	0.31
b	5	2.9	0.37
c	10	5.2	0.36
d	20	14.5	0.42
e	30	22.3	0.45
f	45	30.7	0.47

The particles were packed using a random particle packing algorithm that enables the packing of arbitrarily shaped particles. The algorithm is an extension of principles developed by Jia, Williams (2001) and is part of an ongoing project to develop random packing statistical software (RASPC++). The generic approach involves updating stepwise, the particle positions and rotations in a 3-dimensional box, whilst prohibiting particle-particle overlap. Particle translations and rotations are assigned randomly, though are inclined towards translating towards the bottom of the packing. This phenomenon is governed by a rebounding probability, that is, an upwards movement has to be tested against the probability function for acceptance or rejection. Essentially, the particles have a higher probability of finding an optimal position in the packing process. The algorithm enables the use of any shaped particle, which is achieved by using voxel objects. A voxel is a cubic volume, or, a 3-dimensional pixel. A particle is built up from these equally sized volumes, to form a estimate of the real shape, a higher resolution (voxels per unit length) giving a closer estimate. This strategy caters for trivial collision detection. When moving a particle, all of its voxels are checked to see if they overlap with a voxel from another particle. The approach makes for a highly efficient packing process and there are no limitations on particle geometries. Moreover, since particles fill voxel space, unfilled voxels can easily be summated to calculate the porosity (refer to *Table 1*). Even concave objects, which are practically impossible to pack using an analytical approach, are trivial when using voxel objects. Every voxel was represented using only one single bit packed into a 32 bit word. The effect was a reduction in the magnitude of data consumption to 1/32 as compared to using 32 bits per element in the voxel matrix which allows for the generation of higher resolution packings. Consequently, greater dimensional variance within the packing structure becomes possible to render. More information about the functionalities of RASPC++ can be found in Byholm et al. (2005). Between 3000 and 4000 particles were generated in each packing, which on average required less than a day for completion.

To avoid problems associated with highly resolved data files, numerical output from the packing models was converted to stereolithographic (STL) format, which estimates geometrical surface profiles using triangular arrays. The finalised STL geometry files were output in binary and subsequently uploaded into computational fluid dynamics software, FLOW3D, which was used to conduct the through-packing flow simulations. Flow simulations were carried out in filled systems, that is to say, the entire void space within the packing is filled with fluid. The fluid followed Navier-Stokes equations for incompressible Newtonian flow, *Eqs 2* and *3*. In these equations, ρ is the density, η is the viscosity, p is the pressure, **F** is the volume force field, **u** is a directional velocity and t is the time.

$$\rho\frac{\partial \mathbf{u}}{\partial t}-\eta\nabla^2\mathbf{u}+\rho\left(\mathbf{u}\cdot\nabla\right)\mathbf{u}+\nabla p=\mathbf{F} \qquad [2]$$

$$\nabla\cdot\mathbf{u}=0 \qquad [3]$$

Dimensionless tracers, nine for each simulation, were arranged systematically within the computational grid, after which pressure driven fluid flow simulations ensued. The pressure difference, ΔP, from the top to the bottom of the packing was 100Pa. The fluid material was assigned a viscosity of 0.001Pas. Distances travelled as a function of time were output from the dimensionless tracers in each orthogonal Cartesian axis. These were converted to incremented Euclidean spatial movements and then to the total travelled distance through the packing, L_e, by means of *Eq 4*. In this equation, distances (*x, y, z*) are calculated as a function of the time increments and therefore, smaller time increments would result in a more reliable value for L_e unless the total motion is linear. The integer, *i*, defines the order number of differential increments and $i \leq 1$. Distance increments were collected at every $1 \cdot 10^{-7}$s and in excess of $6 \cdot 10^4$ were used in each simulation. The tortuosity, τ, is then calculated as *Eq 5* where *L* is the shortest vertical distance travelled through the packing media. This computational method for calculating the tortuosity differs somewhat from previous methods as it is not constrained by the computational grid, but rather, by the length of the time increments allowing therefore for lower discretisation resolutions. For example, Armatas (2006), Koponen (1998) and Armatas and Pomonis (2004) calculated tortuosity using distance derivatives based on a rectilinear lattice. D'Arcy permeabilities, *K*, are calculated using *Eq 6*; where η is the fluid viscosity, *A* is the packing area cross section, *q* is the flux, ΔP is the pressure difference between the top and the bottom of the packing and *l* is the distance through the packing. *L* in *Eq 5* is different from *l* in *Eq 6* in that the former is a time dependent distance, which may not have traversed the entire length through the thickness of the packing (defined by *l*).

$$L_e(\mathrm{t})=\sum_i\sqrt{\delta x_i^2(\mathrm{t}_i)+\delta y_i^2(\mathrm{t}_i)+\delta z_i^2(\mathrm{t}_i)} \qquad [4]$$

$$\tau(\mathrm{t})=\frac{L_e(\mathrm{t})}{L(\mathrm{t})} \qquad [5]$$

$$K=\frac{q\cdot\eta\cdot l}{A\cdot\Delta P} \qquad [6]$$

Results and Discussion

Fig 4 shows the mean values calculated for tortuosity, τ, plotted against the packing porosity, φ. Packings using plate-like particles with aspect ratios of 6.52 are plotted separately from plate-like packings using higher aspect ratios (14 and 28). Error bars indicate the standard deviations of τ about the mean.

It is immediately noticeable that τ and φ are inversely proportional to the 1st order for plate-like packings,

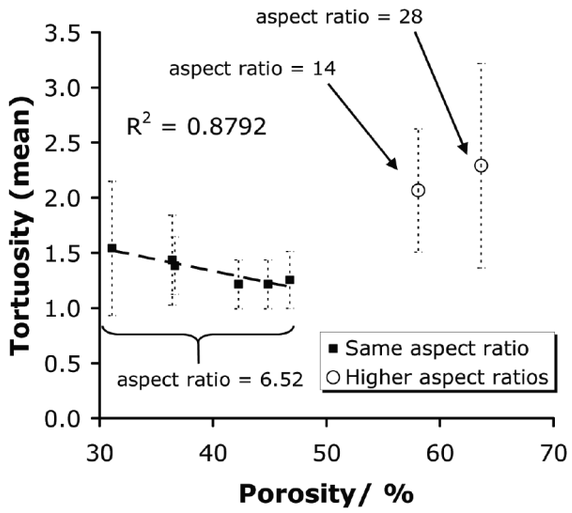

Fig 4. τ plotted against φ for particle packings with different aspect ratios.

provided they all use the same particle aspect ratios. Linear inverse proportionality between τ and φ was also reported by Koponen (1998), who studied non-spherical (square) geometries. This finding is different from the many researchers (e.g. Dias et al. 2006; Kim, Chen 2006; Zalc et al. 2004) who report on an inverse power law trend between τ and φ for spherical packings, suggesting that particle shape is intimately intertwined with porosity to alter the tortuous path. Single monodisperse sphere packings (comprising the same particle volume fraction as the plates) yielded a mean tortuosity value of 1.11. The mean tortuosity values calculated for these plate packings approach this value as a function of an increasing porosity.

Since higher aspect ratio particle packings yield significantly higher τ values, whilst also exhibiting extensive porosity, *Fig 4* furthermore proves that porosity alone is not necessarily the dominating factor in defining the magnitude of the tortuous path. Assuming approximately equal mean particle spatial rotations between the different aspect ratio packings, higher aspect ratio particles yield longer marker-to-plate mean free paths whilst also generating higher pore volumes, a phenomenon that can easily be calculated by integration. *Fig 5* shows a simplified hypothetical pictographic representation of how particle aspect ratios in monodisperse plate packings can increase both the τ and the φ. Tortuosity in porous media saturated with liquid has been determined experimentally by Moldrup et al. (2001). For media comprised of clay minerals and with porosities above 25%, Moldrup and co-workers showed that tortuosity tended to a range between 4 and 2, with a parabolic decline in values for tortuosity as the porosity increased. These values of tortuosity tie in well with the model predictions shown in *Fig 5*, for the plate-like (kaolin clay-type) packings as a function of porosity, which in these models are also saturated with liquid.

The tortuosity of different aspect ratio packings, comprising a similar mean spatial rotation, can additionally be seen to rise linearly as a function of the aspect ratio, *Fig 6*. Higher aspect ratio plates will therefore generate greater lateral tortuous ingress relative to through packing ingress. Consequently, factors such as binder migration and ink spreading-imbibition will follow these paths and quality control factors such as surface ink application can be manipulated by means of the particle aspect ratio.

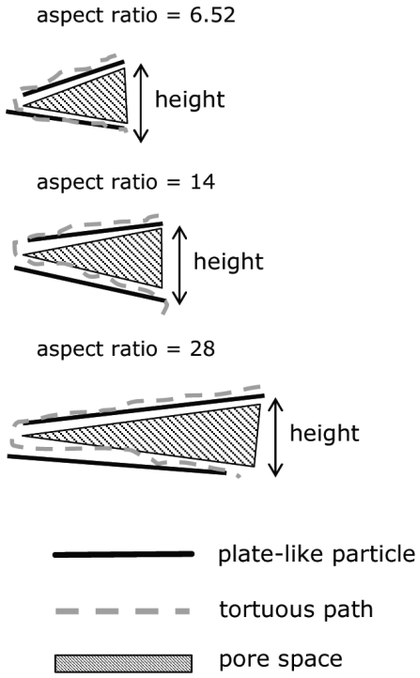

Fig 5. Simplified representation of particle aspect ratio effects on both τ and φ assuming equal maximum heights between the particles. Both τ and φ are hypothetical in this schematic.

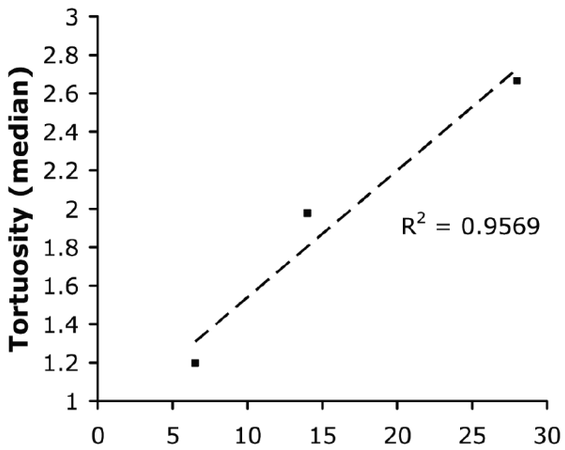

Fig 6. Tortuosity (mean) plotted as a function of the particle aspect ratio.

In *Fig 7*, the tortuosity for each tracer is plotted against corresponding mean tracer velocity values, ε. Two linear lines are applied to the points to show that higher tortuosity values are always accompanied by lower mean tracer velocities. The expanded section of the graph focuses on τ≤2 and shows inversely linear proportionality with ε. Higher scatter about the linear regression line can be observed as τ increases and ε decreases. This phenomenon, as well as the extremely high values for tortuosity seen in *Fig 7* can be attributed to the existence of nesting sites for local fluid material. Nesting sites are essentially cavities that trap the through-packing flux of the fluid material but without necessarily trapping lateral move-

ment. Such cavities arise as a function of the particle geometry coupled with the packing arrangement. As the depth of the cavity increases, the likelihood of fluid escape from the cavity progressively decreases. The result is that the tracers that are fully nested will move laterally for any length of input time, but will never progress beyond a particular packing depth. This significantly magnifies the 'true' value for tortuosity. Tracers may also experience partial nesting, that is, they escape from cavities after having spent time in them. The result of such a phenomenon is that partially nested tracers will exhibit considerably lower mean velocities and account for the higher levels of τ-ε scatter at lower values of ε. It is also perfectly plausible that if nesting does not occur, tracer velocities are reduced on impacting particles through the packing. An impact occurring on the edge of a particle indicates that the tracer would not have travelled a great distance, but would still lose its velocity. Contrarily, impaction closer to the middle of a particle results in a higher distance travelled with a low tracer velocity. *Fig 8* shows a 2-dimensional theoretical pictograph of both nesting and non-nesting mechanisms that lead to high scatter in the range of low tracer velocities.

The mean value of τ is plotted in *Fig 9* against the mean spatial rotation, ω_t for packings (a)-(f). The error bars indicate the standard deviations about the mean. In this figure, there appears to be no apparent trend between the tortuosity of a packing and the mean spatial rotation of the particles within the packing. It is quite plausible that since tortuosity is highly localised, the use of local rather than mean spatial rotations would be more informative.

In *Fig 10*, mean values of τ are plotted against -ln(K) for corresponding packings. According to Wang et al. (2005), who analysed materials with permeability constants ranging over three orders of magnitude, tortuosity and permeability are inversely related properties. The results from *Fig 10* therefore indicate a similar exponentially decreasing tendency between τ and K for the computationally packed plate-like packings.

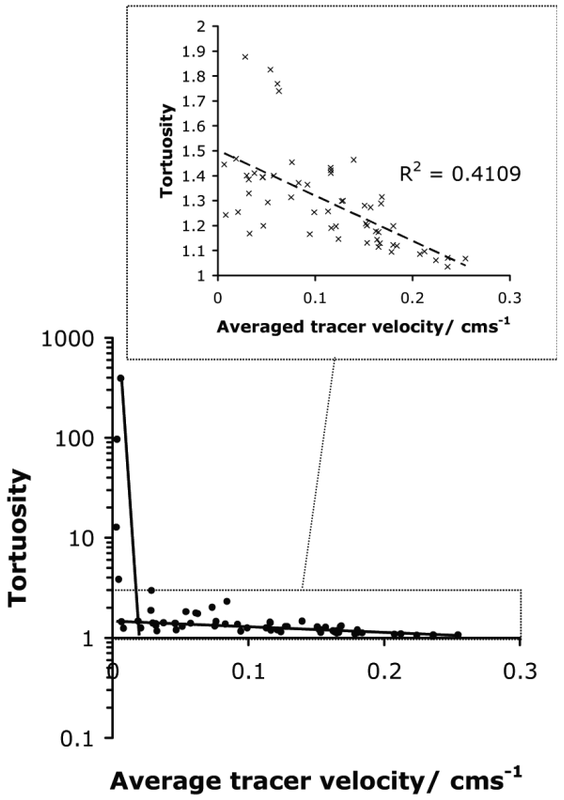

Fig 7. Tracer tortuosity plotted against corresponding mean tracer velocity values.

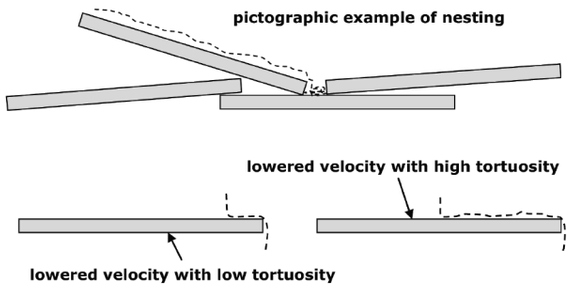

Fig 8. 2-dimensional pictographic representation of nesting. The dotted line represents a dimensionless tracer following the movement of fluid.

Conclusions

Anfractuous materials have been computationally generated out of quasi-randomly packed plate-like particles for the purpose of calculating the fluid flow tortuosity. Plate-like particle packings show a rise in porosity as a function of increasing the mean Euclidean spatial rotations. Though tortuosity is inversely proportional to the porosity, any trend with respect to the mean spatial rotation is unclear. It is possible that a comparison to localised spatial rotations would be more informative, however, currently; this is beyond the scope of the research undertaken herein. The inversely proportional relationship between tortuosity and porosity in monodisperse plate-like particle packings is somewhat different to parabolic trends often reported for spherical packings. It would seem that this difference is an attribute of the particle geometry and the consequent packing structure. Microstructure design using plate-like particles

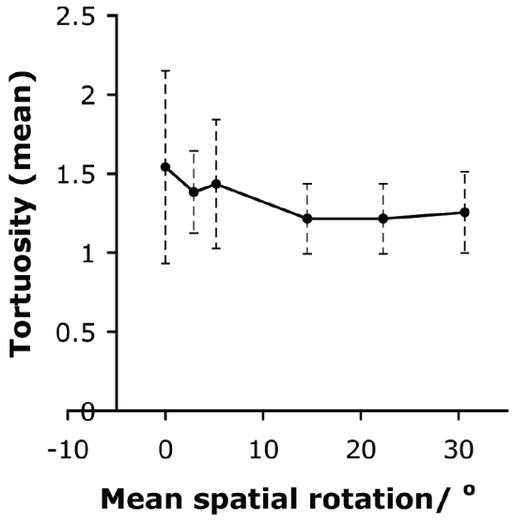

Fig 9. Mean τ plotted as a function of the mean spatial rotation, ω_t.

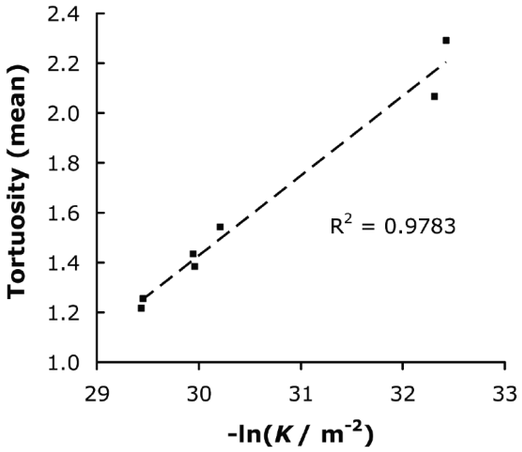

Fig 10. Mean τ plotted as a function -ln(*K*).

should therefore take into consideration that the rate of change is constant between tortuosity and porosity, rather than exponential as observed in spherical packings. If the aspect ratio is increased, the tortuous path is lengthened and porosity shows less dominance relative to plate aspect ratio as a determinant of tortuosity. This postulation is made because higher porosity packings also comprising higher aspect ratio particles yielded significantly higher value of tortuosity. In order to enhance barrier performance therefore, the use of higher aspect ratio particles would lessen the dependence on minimising the porosity.

Tracer particle velocities are related to tortuosity alongside nesting phenomena. It is hypothesised that lower velocities coupled with higher degrees of variance is a consequence of either full or partial nesting. Furthermore, repeated impaction of tracers with particles can result in reduced velocities even though the tortuous path travelled is not high. Ultimately, the scatter in tortuosity coupled with low tracer velocities is a function of where on each particle the tracer happens to impact. Tortuosity shows no relationship as a function of the mean spatial rotation angle. Since the tortuous path is highly localised, it is possible that it would be better to make the comparison with more local spatial rotations. There exists nevertheless, linear proportionality of tortuosity as a function of the natural logarithm of the D'Arcy permeability. Therefore, the tortuosity can be said to decrease exponentially as a function of an increasing permeability. Essentially, increasing the tortuosity of plate-like packings can be controlled to generate a less permeable structure, which can be useful in enhancing the barrier properties of coatings.

Porous structures subjected to an external pressure are essentially deformable. This time dependent deformation gives rise to reduced pore dimensions and somewhat changes the extent of the tortuous path. The work performed herein has focused on non-deformable structures but has used low application pressures to generate fluid flow. The research reported in this paper contributes a small step towards further understanding tortuosity-microstructure relationships in plate-like particle packings.

Literature

Allaire-Leung, S.E., Gupta, S.C. and Moncrief, J.F. (2000): Water and solute movement in soil as influenced by macropore characteristics 2. macropore tortuosity, J. Contam. Hydrol. 41, 303.

Armatas, G.S. (2006): Determination of the effects of the pore size and pore connectivity distribution on the pore tortuosity and diffusive transport in model porous networks, Chem. Eng. Sci. (accepted manuscript).

Armatas, G.S. and Pomonis, P.J. (2004): A Monte Carlo pore network for the simulation of porous characteristics of functionalized silica: pore size distribution, connectivity distribution and mean tortuosities, Chem. Eng. Sci. 59, 5735.

Attia, A.M. (2005): Effects of petrophysical rock properties on tortuosity factor, J. Pet. Sci. Eng. 48, 185.

Bear, J. (1972): Dynamics of fluids in porous media, Elsevier, New York.

Boudreau, B.P. (1996): The diffusive tortuosity of fine-grained unlithified sediments, Geochim. Cosmochim. Acta 60(16), 3139.

Byholm, T., Alam, P., Sinervo, L., Stoor, C. and Toivakka, M. (2005): The use of 3-dimensional image analysis and computer simulation for gathering statistical data and physical constants for paper coating, PTS Coating Symposium, Baden-Baden, Germany.

Cumberland, D.J. and Crawford, R.J. (1987): The packing of particles, Handbook of Powder Technology – Volume 6, Elsevier Science Publishers B. V., Netherlands, p. 98.

Dias, R., Teixeira, J.A., Mota, M. and Yelshin, A. (2006): Tortuosity variation in a low density binary particulate bed, Sep. Purif. Technol. (article in press).

Dullien, F.A.L. (1992): Fluid transport and pore structure, 2nd Ed., Academic Press Inc., San Diego, CA.

Epstein, N. (1989): On tortuosity and the tortuosity factor in flow and diffusion through porous media, Chem. Eng. Sci. 44, 777.

Jia, X. and Williams, R.A. (2001): A packing algorithm for particles of arbitrary shapes, Powder Technol. 120, 175.

Kim, A.S. and Chen H. (2006): Diffusive tortuosity factor of solid and soft cake layers: a random walk simulation approach, J. Membr. Sci. (article in press).

Koponen, A. (1998): Simulations of fluid flow in porous media by lattice-gas and lattice-Boltzmann mathos, Ph.D. Thesis, University of Jyväskyla, Jyväskylä, Finland.

Maerki, M., Wehrli, B., Dinkel, C. amd Müller, B. (2003): The influence of tortuosity on molecular diffusion in freshwater sediments of high porosity, Geochim. Cosmochim. Acta 68(7), 1519.

Moldrup, P., Olesen, T., Komatsu, T. Schjønning, P and Rolston, D.E. (2001): Tortuosity, diffusivity and permeability in the soil liquid and gaseous phases, Soil. Sci. Am. J. 65, 613.

Petford, N. and Koenders, M. A. (2000): Consolidation phenomena in sheared granitic magma: effects of grain size and tortuosity, Phys. Chem. Earth (A) 26(4-5), 281.

Wang, R., Pavlin, T., Rosen, M.S., Mair, R.W., Cory, D.G. and Walsworth, R.L. (2005): Xenon NMR measurements of permeability and tortuosity in reservoir rocks, Magnetic Resonance Imaging, 23 329.

Zalc, J. M., Reyes, S.C. and Iglesia, E. (2004): The effects of diffusion mechanism and void structure on transport rates and tortuosity factors in complex porous structures, Chem. Eng. Sci. 59, 2947.

Manuscript received May 19, 2006
Accepted September 13, 2006